

DNA REPAIR

Stochastic activation of a DNA damage response causes cell-to-cell mutation rate variation

Stephan Uphoff,^{1,2*} Nathan D. Lord,² Burak Okumus,² Laurent Potvin-Trottier,^{2,3} David J. Sherratt,¹ Johan Paulsson^{2*}

Cells rely on the precise action of proteins that detect and repair DNA damage. However, gene expression noise causes fluctuations in protein abundances that may compromise repair. For the Ada protein in *Escherichia coli*, which induces its own expression upon repairing DNA alkylation damage, we found that undamaged cells on average produce one Ada molecule per generation. Because production is stochastic, many cells have no Ada molecules and cannot induce the damage response until the first expression event occurs, which sometimes delays the response for generations. This creates a subpopulation of cells with increased mutation rates. Nongenetic variation in protein abundances thus leads to genetic heterogeneity in the population. Our results further suggest that cells balance reliable repair against toxic side effects of abundant DNA repair proteins.

The integrity of the genome is constantly threatened by DNA damage. Most damage events are reversed by active repair systems, but the ones that escape repair can cause cell death or mutations. An intriguing question is what causes those failures. Specifically, the classic perspective suggests that failures to repair reflect the intrinsic error rate of the repair enzymes, for example, because of the random search for lesions (1, 2). Alternatively, most failures could occur in an error-prone subpopulation of cells (3, 4) in which repair is compromised by fluctuations in the abundances of the repair proteins (5–7).

To distinguish between these possibilities we quantitatively analyzed, with single-molecule resolution in single cells, the adaptive response that protects *Escherichia coli* against the toxic and mutagenic effects of DNA alkylation damage (8). The Ada protein functions not only in the direct repair of alkylated DNA but also as the transcriptional activator of the adaptive response (Fig. 1A) (9, 10). Specifically, *ada* expression is induced by methylated Ada (meAda) after irreversible methyl transfer from DNA phosphotriester and O⁶MeG lesions onto cysteine residues of Ada. Because Ada is present in low numbers before damage, this positive-feedback gene regulation may amplify stochastic fluctuations and create cell-to-cell heterogeneity in the repair system (2, 11).

We imaged the endogenous expression of a functional Ada-mYPet fluorescent protein fusion (fig. S1), in cells treated with methyl methanesulfonate (MMS) (Fig. 1B). We observed a strong and uniform expression of Ada in most cells, but

20% of the cells did not respond at all, even at saturating doses of MMS (Fig. 1, B and C). Quantitatively similar results were obtained with a transcriptional fluorescent reporter in cells with untagged Ada (fig. S2), which showed that the protein fusion did not affect the observations.

To visualize the dynamics of the process, we monitored Ada-mYPet abundance in real time in a microfluidic device that allows imaging of single cells over tens of generations during constant DNA damage treatment (fig. S3 and movies S1 and S2) (12, 13). At low-to-intermediate MMS concentrations (<200 μM MMS), cells showed random unsynchronized pulses of Ada expression (Fig. 1D). The pulse frequency increased proportionally to the MMS concentration (fig. S4), as expected when triggering is limited by the probability that Ada finds a lesion. At higher MMS concentrations, most cells rapidly induced a persistent and uniform response (Fig. 1E). However, 20 to 30% of cells were lagging even at saturating MMS and triggered the response after exponentially distributed delays with an average of one generation time (Fig. 1F and fig. S5). Some cells thus failed to respond for several generations.

To identify the molecular determinants of this heterogeneity, we measured the Ada abundance before MMS treatment. Ada-mYPet was undetectable over the autofluorescence background of cells, which suggested that absolute amounts were on the order of a few molecules per cell. We therefore turned to single-molecule microscopy to directly count individual proteins in live cells (Fig. 1G and fig. S6). The abundance of Ada was extremely low: The observed population average was 1.4 ± 0.1 molecules per cell (\pm SEM) and 20 to 30% of the cells did not contain a single Ada molecule. Because the *ada* gene is strictly autoregulatory, i.e., it can only be induced by the Ada protein (8–10, 14), cells with zero Ada molecules should be unable to trigger the adaptive response, despite great amounts of damage. This is supported by

the quantitative agreement between the percentages of cells with a delayed response and with zero Ada molecules. Consequently, the delay before response activation should match the time until the first random expression event occurs in these cells. Indeed, the distribution of Ada copies before damage was very close to a Poisson distribution (Fig. 1G) with an average production rate of one molecule per cell cycle (fig. S6), and the late-responding cells also activated the response with a Poisson rate of once per cell cycle (Fig. 1F).

These findings also mean that most cells reliably launch the response with just one or two Ada molecules to sense the damage and to induce *ada* expression (Fig. 2A). We indeed observed distinct single-molecule signatures: The rates of Ada production displayed staircase patterns with equidistant states during response activation and deactivation at low MMS concentrations (Fig. 2B and fig. S7), indicative of discrete production and loss events of the meAda molecules that control Ada expression. To further confirm the low numbers, we titrated meAda using promoter sites on a low copy-number plasmid (15), which markedly decreased steady-state Ada induction, as expected (fig. S8). Furthermore, the discrete production rate steps disappeared when meAda abundance was increased using high MMS concentrations (fig. S7).

Because failure to trigger the adaptive response seems to be the result of a complete lack of Ada molecules in a fraction of cells, it should be possible to reduce this fraction with a slight increase in the average abundance of Ada. Specifically, for many distributions (including the Poisson) the probability mass in the tails depends sensitively on the average. We therefore moderately increased Ada numbers per cell either by inhibiting cell division—keeping the concentrations constant (16)—or by expressing additional unlabeled Ada from the P_{Ada} promoter on a very low copy-number plasmid (MiniF; ~2 copies per cell). In both cases, we observed the predicted uniform MMS response and disappearance of the late-responding cell subpopulation (Fig. 2, C and D).

These observations raise the question of why the native *ada* gene is expressed at such low basal amounts. Following the fates of single cells over time showed that a failure to activate the adaptive response during MMS treatment lowered the viability of those cells, as expected (Fig. 3A and fig. S9). However, the moderate overexpression of Ada resulted in severe toxicity of MMS treatment (Fig. 3A and fig. S10) (14, 17) and caused spontaneous triggering of the response in the absence of MMS (Fig. 3B and fig. S10), something we never observed at native *ada* expression (Fig. 3B and fig. S3). The extremely low abundance of Ada can thus be advantageous to the population as a whole, which implies that the repair system faces a trade-off to repair exogenous alkylation damage without introducing harmful effects. In fact, given the low numbers of molecules, the *ada* regulation is remarkably precise: First, the Poisson distribution before damage shows an almost complete absence of gene expression bursts or “extrinsic” noise (Fig. 3C and fig. S6), in stark contrast to the regulation

¹Department of Biochemistry, University of Oxford, Oxford OX1 3QU, UK. ²Department of Systems Biology, Harvard Medical School, Boston, MA 02115, USA. ³Biophysics Ph.D. Program, Harvard Medical School, USA.

*Corresponding author. E-mail: stephan.uphoff@bioch.ox.ac.uk (S.U.); johan_paulsson@harvard.edu (J.P.)

of most genes studied (5, 6, 7, 18). This can be explained by a short half-life and inefficient translation of *ada* mRNAs (19, 20), as well as the tendency of Poisson noise to dominate at very low abundances. Second, a dual reporter assay (5) that simultaneously monitors expression of the endogenous P_{Ada} *ada*-mYPet and an ectopic P_{Ada} *cfp* insertion (Fig. 3, D and E, and fig. S11) showed that both the activation time after MMS treatment and the subsequent expression dynamics were closely correlated between the two genes, with little uncorrelated noise that would indicate transcriptional bursting. Considering the central role of meAda in *ada* regulation (8–10, 14), these expression dynamics likely reflect fluctuations in meAda numbers. Indeed, the normalized standard deviation was inversely proportional to the square root of the expected average number of DNA damage sites, quantitatively consistent with the simplest model, where varying damage levels determine meAda abundances that then reliably control *ada* expression (fig. S12). Third, *ada* transcription activation is inhibited by unmethylated Ada. This may

control response deactivation after the damage has been repaired (21). Indeed, removal of MMS caused all cells to switch off the adaptive response uniformly, and Ada was diluted because of cell growth (Fig. 3F).

The total number of Ada molecules directly determines a cell's repair capacity: each Ada molecule can only act once to remove one mutagenic O^6 MeG lesion (10). Furthermore, a lack of Ada repair capacity cannot be compensated for by the DNA mismatch repair pathway, because unrepaired O^6 MeG lesions miscode for T instead of C. This leads to futile mismatch repair cycles, which eventually cause stable mutations during the next round of replication (17). We therefore tested whether heterogeneity in Ada concentrations affects mutation rates. To directly measure genomic mutation rates in single cells, we used the DNA mismatch recognition protein MutS as a marker for labeling nascent mutations (22). Specifically, photoactivated single-molecule tracking (23) allowed us to classify individual MutS-PAmCherry fusion proteins as DNA-bound or mobile (24, 25),

while also imaging Ada-mYPet in the same live cells (Fig. 4). Without MMS treatment, the apparent mutation frequency was low (fig. S13), and most MutS molecules were mobile (average 6% bound) (fig. S14). MMS treatment of Ada-deficient cells (Δada) increased both the mutation frequency (fig. S13) and MutS binding (56% bound) (Fig. 4 and fig. S14). MMS treatment of wild-type cells resulted in highly variable amounts of bound MutS molecules between cells. This variation could be entirely explained by the heterogeneity in Ada expression (Fig. 4 and fig. S15): MutS binding was increased only in the subpopulation of cells with low Ada expression (30% bound), whereas cells with abundant Ada retained low MutS activity (10% bound). Stochastic activation of the adaptive response therefore leads to an error-prone cell subpopulation that does not efficiently repair DNA alkylation damage and accumulates mutations.

We found that a cell's fate after DNA damage can be accurately predicted by the presence or absence of a single protein molecule. The resulting cell heterogeneity increases the chance

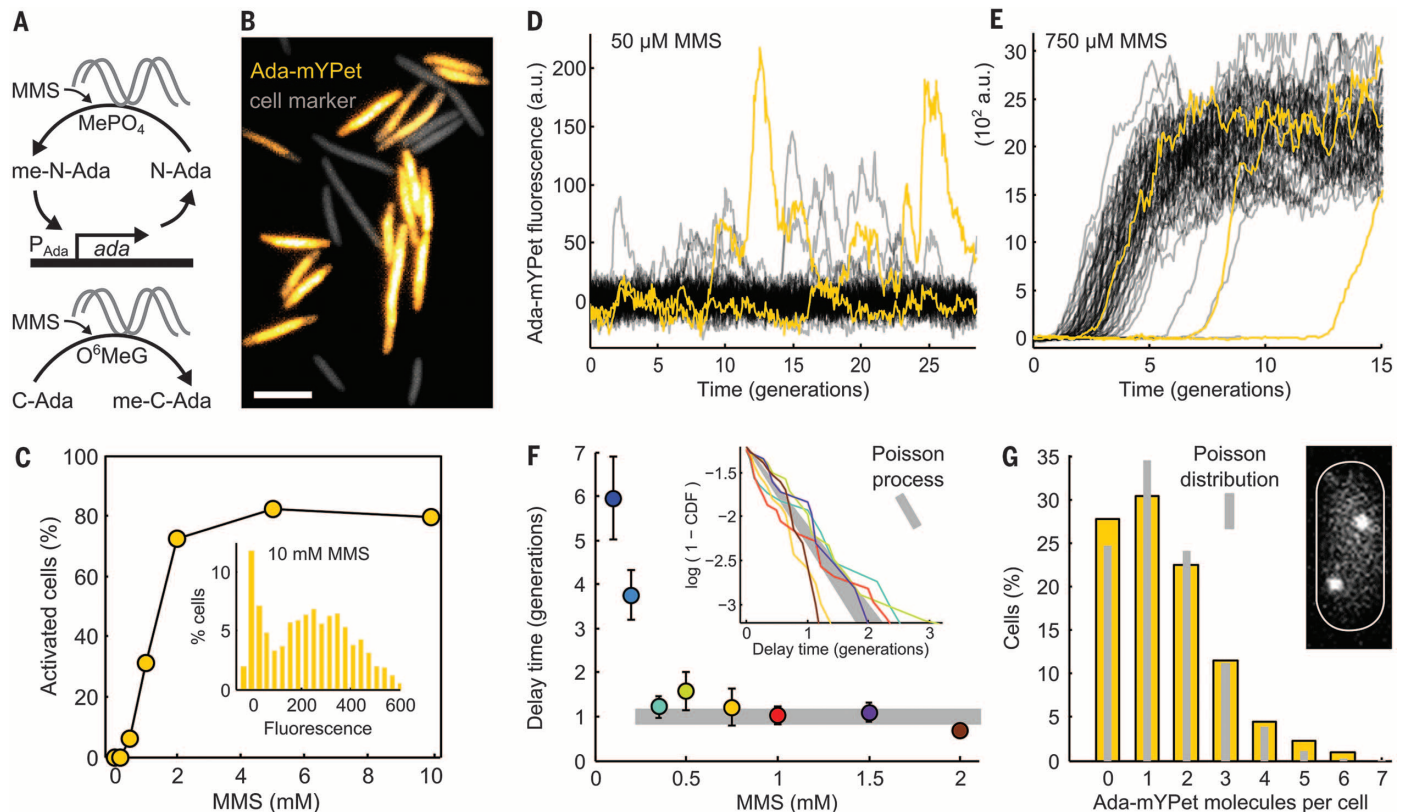
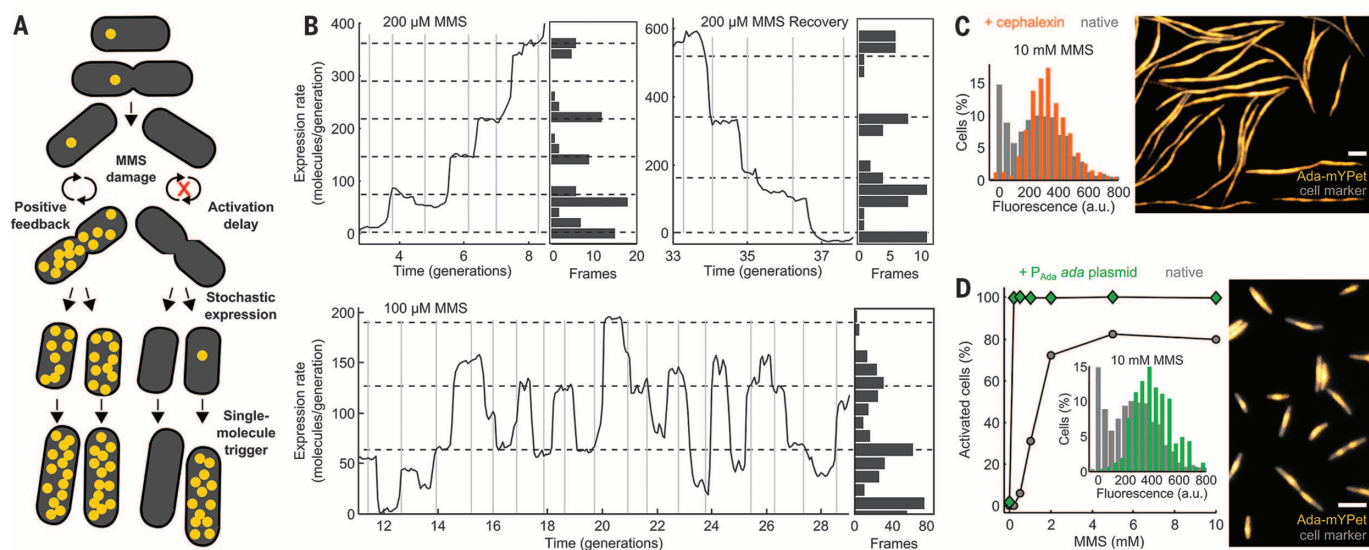


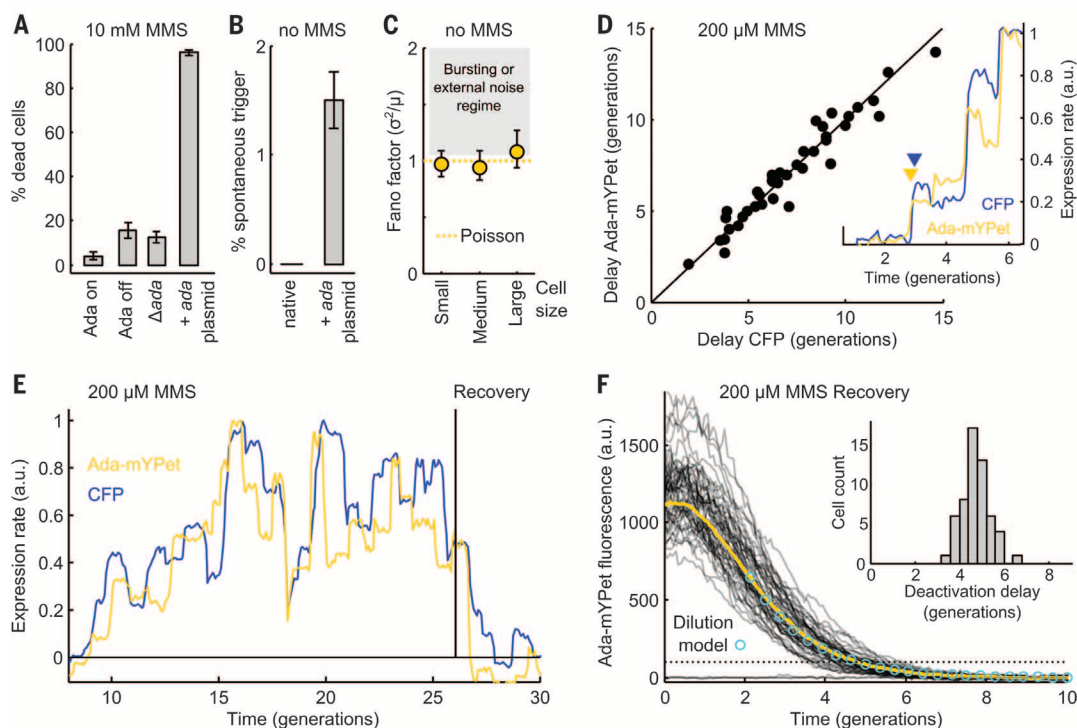
Fig. 1. Stochastic gene expression delays Ada response activation in a cell subpopulation. (A) Methylation of Ada N- and C-terminal domains functions as a damage sensor, turning Ada into an autoregulatory activator of genes involved in DNA alkylation repair. (B) Ada-mYPet fluorescence (yellow) in cells treated with 10 mM MMS for 1 hour. Constitutive mKate2 serves as fluorescent cell marker (gray). Scale bar, 5 μ m. (C) Percentage of cells that activated Ada-mYPet expression after 1 hour in MMS. (Inset) Histogram of Ada-mYPet fluorescence per cell with 10 mM MMS. (D and E) Time traces of Ada-mYPet fluorescence in single cells treated with 50 μ M and 750 μ M MMS (added at time 0). Example cells in yellow; time in units of average generation times (42 min) throughout. (F) (Inset) Transformed cumulative distribution

log(1-CDF) of response delay times for the last 30% of cells to activate Ada-mYPet expression after MMS treatment in the microfluidic chip. Different MMS concentrations in colors as in main plot. Straight lines on log scale reflect exponential distributions as generated by a Poisson process; the slope corresponds to the average-delay time constant. Gray area: Poisson process with a rate of 1 ± 0.1 per generation. Main plot: Average delay time constants from the inset data (\pm SEM). (G) Single-molecule counting of Ada-mYPet without MMS. Example cell shown. Poisson model was generated using measured production rate of 1 molecule per generation. Note that the actual value may be closer to 1.2 because of delayed maturation of mYPet (see supplementary materials).



Histograms show number of frames spent in the expression rate states. Losses can occur because of rare meAda degradation or by segregation at cell division. At very low numbers, all meAda molecules should sometimes remain in the same cell, maintaining expression rates, as observed. (C) Uniform Ada-mYPet induction when cell division was inhibited with cephalaxin before MMS treatment (orange). (D) Uniform accumulation of endogenous Ada-mYPet with additional MiniF plasmid carrying P_{Ada} *ada* (green). Scale bars, 5 μ m.

Histograms show number of frames spent in the expression rate states. Losses can occur because of rare meAda degradation or by segregation at cell division. At very low numbers, all meAda molecules should sometimes remain in the same cell, maintaining expression rates, as observed. (C) Uniform Ada-mYPet induction when cell division was inhibited with cephalaxin before MMS treatment (orange). (D) Uniform accumulation of endogenous Ada-mYPet with additional MiniF plasmid carrying P_{Ada} *ada* (green). Scale bars, 5 μ m.



activation for endogenous *ada-mYPet* and ectopic P_{Ada} *cfp* are closely correlated. Each dot represents one cell. (Inset) Example expression-rate time traces with simultaneous activation of both genes. (E) Example time traces showing correlated expression-rate fluctuations of the dual reporter genes and simultaneous response deactivation after MMS removal. (F) Deterministic response deactivation: Time traces after MMS removal at time 0 (average: yellow). The dilution model (circles) has an exponential decay constant equal to the average generation time. (Inset) Narrow distribution of delay times from MMS removal until response is deactivated (dotted line threshold).

activation for endogenous *ada-mYPet* and ectopic P_{Ada} *cfp* are closely correlated. Each dot represents one cell. (Inset) Example expression-rate time traces with simultaneous activation of both genes. (E) Example time traces showing correlated expression-rate fluctuations of the dual reporter genes and simultaneous response deactivation after MMS removal. (F) Deterministic response deactivation: Time traces after MMS removal at time 0 (average: yellow). The dilution model (circles) has an exponential decay constant equal to the average generation time. (Inset) Narrow distribution of delay times from MMS removal until response is deactivated (dotted line threshold).

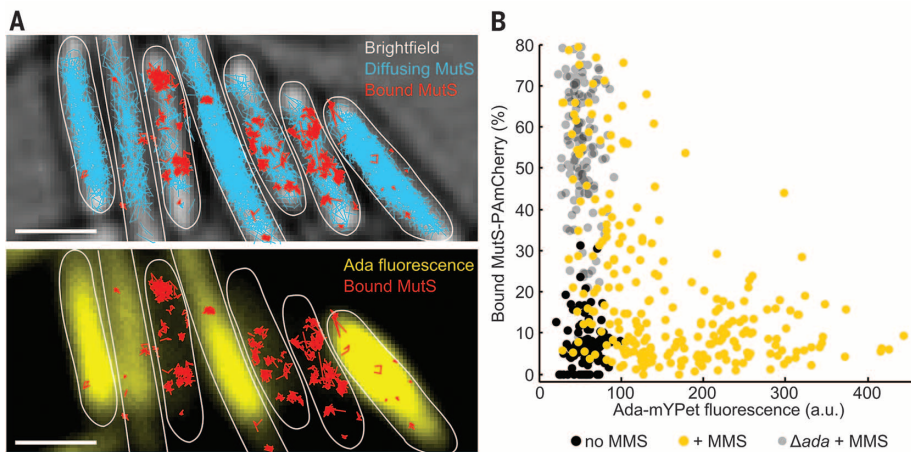


Fig. 4. Increased binding of mismatch recognition protein MutS in cells with delayed Ada response. Photoactivated single-molecule tracking of MutS-PAmCherry and Ada-mYPet fluorescence in single cells treated with 10 mM MMS for 1 hour. **(A)** Tracks of bound (red) and mobile MutS (blue). Cell outlines drawn; scale bars, 2 μm . **(B)** Percentage of bound MutS molecules versus Ada-mYPet fluorescence per cell. Native strain with (yellow) and without MMS (black); Δada with MMS (gray).

of genetic adaptation in a hypermutagenic subpopulation of cells without jeopardizing the genetic integrity in the majority of the population during stress (3, 26). However, our observations that high Ada expression is toxic and that cells appear to minimize the heterogeneity in several ways suggest that this is not an adaptive bet-hedging strategy, but rather a side effect of maximizing short-term fitness: Because proteins with the capacity to modify DNA can be detrimental, cells may be forced to express them in low amounts, such that random fluctuations are unavoidable. Mutations can then result from stochastic variation in the concentrations of DNA repair proteins. Just as genetic heterogeneity can cause phenotypic heterogeneity, the reverse is thus also true.

REFERENCES AND NOTES

1. N. M. Kad, B. Van Houten, *Prog. Mol. Biol. Transl. Sci.* **110**, 1–24 (2012).

2. S. Uphoff, A. N. Kapanidis, *DNA Repair (Amst.)* **20**, 32–40 (2014).
3. R. S. Galhardo, P. J. Hastings, S. M. Rosenberg, *Crit. Rev. Biochem. Mol. Biol.* **42**, 399–435 (2007).
4. A. Marusyk, V. Almendro, K. Polyak, *Nat. Rev. Cancer* **12**, 323–334 (2012).
5. M. B. Elowitz, A. J. Levine, E. D. Siggia, P. S. Swain, *Science* **297**, 1183–1186 (2002).
6. I. Golding, J. Paulsson, S. M. Zawilski, E. C. Cox, *Cell* **123**, 1025–1036 (2005).
7. P. J. Choi, L. Cai, K. Frieda, X. S. Xie, *Science* **322**, 442–446 (2008).
8. L. Samson, J. Cairns, *Nature* **267**, 281–283 (1977).
9. P. Landini, M. R. Volkert, *J. Bacteriol.* **182**, 6543–6549 (2000).
10. B. Sedgwick, *Nat. Rev. Mol. Cell Biol.* **5**, 148–157 (2004).
11. U. Alon, *Nat. Rev. Genet.* **8**, 450–461 (2007).
12. P. Wang *et al.*, *Curr. Biol.* **20**, 1099–1103 (2010).
13. T. M. Norman, N. D. Lord, J. Paulsson, R. Losick, *Nature* **503**, 481–486 (2013).
14. D. E. Shevell, P. K. LeMotte, G. C. Walker, *J. Bacteriol.* **170**, 5263–5271 (1988).
15. R. C. Brewster *et al.*, *Cell* **156**, 1312–1323 (2014).
16. J. C. W. Locke, J. W. Young, M. Fontes, M. J. Hernández Jiménez, M. B. Elowitz, *Science* **334**, 366–369 (2011).

17. D. Fu, J. A. Calvo, L. D. Samson, *Nat. Rev. Cancer* **12**, 104–120 (2012).
18. H. Maamar, A. Raj, D. Dubnau, *Science* **317**, 526–529 (2007).
19. J. A. Bernstein, A. B. Khodursky, P.-H. Lin, S. Lin-Chao, S. N. Cohen, *Proc. Natl. Acad. Sci. U.S.A.* **99**, 9697–9702 (2002).
20. G.-W. Li, D. Burkhardt, C. Gross, J. S. Weissman, *Cell* **157**, 624–635 (2014).
21. B. M. Sage, G. C. Walker, *Proc. Natl. Acad. Sci. U.S.A.* **91**, 9730–9734 (1994).
22. M. Elez *et al.*, *Curr. Biol.* **20**, 1432–1437 (2010).
23. S. Manley *et al.*, *Nat. Methods* **5**, 155–157 (2008).
24. S. Uphoff, R. Reyes-Lamothé, F. Garza de Leon, D. J. Sherratt, A. N. Kapanidis, *Proc. Natl. Acad. Sci. U.S.A.* **110**, 8063–8068 (2013).
25. Y. Liao, J. W. Schroeder, B. Gao, L. A. Simmons, J. S. Biteen, *Proc. Natl. Acad. Sci. U.S.A.* **112**, E6898–E6906 (2015).
26. J.-W. Veening, W. K. Smits, O. P. Kuipers, *Annu. Rev. Microbiol.* **62**, 193–210 (2008).

ACKNOWLEDGMENTS

We thank R. Reyes-Lamothé, U. Alon, J.-Y. Bouet, A. Kapanidis, C. Lesterlin, A. Upton, and P. Zawadzki for reagents and discussions. We thank C. Saenz and the Microfluidics Core Facility at Harvard Medical School. Microscopy at Micron Oxford was supported by a Wellcome Trust Strategic Award (091911) and Medical Research Council grant (MR/K01577X/1). S.U. is funded by a Sir Henry Wellcome Fellowship by the Wellcome Trust and a Junior Research Fellowship at St John's College, Oxford. J.P., N.D.L., L.P.-T., and B.O. are funded by NIH grant GM095784. L.P.-T. acknowledges fellowship support from the Natural Sciences and Engineering Research Council of Canada (NSERC) and the Fonds de recherche du Québec-Nature et technologies. D.J.S. is funded by a Wellcome Trust Investigator Award (099204/Z/12Z). The primary data described in the manuscript is available upon request. Author contributions: S.U. conceived the study, generated cell strains, and designed and performed experiments and analysis. S.U., D.J.S., and J.P. interpreted the data. N.L. and L.P.-T. developed the microfluidic imaging methods. B.O. developed the single-molecule counting method. S.U., D.J.S., and J.P. wrote the manuscript. The authors declare competing financial interests. A U.S. Patent Application 20150247790 entitled "Microfluidic assisted cell screening" was filed on behalf of B.O., J.P., and co-workers by the President and Fellows of Harvard College.

SUPPLEMENTARY MATERIALS

www.sciencemag.org/content/351/6277/1094/suppl/DC1
Materials and Methods
Figs. S1 to S15
Table S1
Movies S1 and S2
References (27–35)

8 July 2015; accepted 5 February 2016
10.1126/science.aac9786



Stochastic activation of a DNA damage response causes cell-to-cell mutation rate variation

Stephan Uphoff *et al.*
Science **351**, 1094 (2016);
DOI: 10.1126/science.aac9786

This copy is for your personal, non-commercial use only.

If you wish to distribute this article to others, you can order high-quality copies for your colleagues, clients, or customers by [clicking here](#).

Permission to republish or repurpose articles or portions of articles can be obtained by following the guidelines [here](#).

The following resources related to this article are available online at www.sciencemag.org (this information is current as of March 31, 2016):

Updated information and services, including high-resolution figures, can be found in the online version of this article at:
</content/351/6277/1094.full.html>

Supporting Online Material can be found at:
</content/suppl/2016/03/02/351.6277.1094.DC1.html>

This article **cites 35 articles**, 12 of which can be accessed free:
</content/351/6277/1094.full.html#ref-list-1>

This article appears in the following **subject collections**:
Cell Biology
/cgi/collection/cell_biol